Biophysical Journal Volume 72 March 1997 1092–1108

Biophysical and Functional Consequences of Receptor-Mediated Nerve Fiber Transformation

Darrell L. Tanelian and Vladislav S. Markin
The Eugene McDermott Center for Pain Management, Department of Anesthesiology and Pain Management, University of Texas Southwestern Medical Center, Dallas, Texas 75235-9068 USA

ABSTRACT Stimulation of the nervous system by substance P, a G protein-coupled receptor, and subsequent receptor internalization causes dendrites to change their shape from homogeneous cylinders to a heterogeneous string of swollen varicosities (beads) connected by thin segments. In this paper we have analyzed this phenomenon and propose quantitative mechanisms to explain this type of physical shape transformation. We developed a mathematical solution to describe the relationship between the initial radius of a cylindrical nerve fiber and the average radii of the subsequently created varicosities and connecting segments, as well as the periodicity of the varicosities along the nerve fiber. Theoretical predictions are in good agreement with our own and published experimental data from dorsal root ganglion neurons, spinal cord, and brain. Modeling the electrical properties of these beaded fibers has led to an understanding of the functional biophysical consequences of nerve fiber transformation. Several hypotheses for how this shape transformation can be used to process information within the nervous system have been put forth.

INTRODUCTION

Varicosities along small axonal or dendritic processes in the nervous system have been described since the time of Ramon y Cajal (1952, 1955) when he observed varicosities along a variety of neural processes, including corneal nerve terminals and various sites in sympathetic ganglia, cerebellum, and hippocampus. Since these initial observations, a variety of different treatments have been shown to induce varicosity formation along neuronal processes, although little is known of their functional significance (Fig. 1).

Varicosity formation has been induced in neurites of cultured dorsal root ganglion (DRG) cells after exposure to lidocaine (2.25×10^{-3} M) or procaine (2×10^{-3} M). This effect was most pronounced after 3–4 h of exposure to either local anesthetic (Anderson and Bamburg, 1981). Exposure to the neurotoxin *n*-hexane (10–60 ng/ml) resulted in marked varicosity formation in DRG neurites within 30 min of administration (Stoltennbury-Didinger, 1992). The possibility that cytoskeletal proteins are involved in varicosity formation arises from the data of Meller (1992). In that study administration of cytochalasin B (10 μg/ml), which depolymerizes actin, caused varicosity formation in DRG processes. Additionally, administration of colchicine (10 μg/ml), which prevents the assembly of tubulin into microtubules, or an antibody against a 68-kDa neurofilament protein were also shown to induce varicosity formation.

Traumatic stimulation is known to cause varicosity formation in DRG processes. In an extreme example of this effect, Bird (1978) showed varicosity formation in transected DRG processes within 30 min of transection. Suneson et al. (1989) showed that exposure of DRG cultures to short-duration, high-energy, mechanical stimulation elicits marked changes in neural varicosities, which became more irregular in spacing and size. This study indicates that traumatic mechanical stimulation may result in a change in the pattern of varicosities found in DRG processes.

Recently it has been shown in vivo that somatosensory stimulation induces varicosity formation in distal dendrites (<4 μm in diameter) of lamina I spinal cord neurons (Mantyh et al., 1995a,b). Mantyh et al. reported that either paw pinch or capsaicin injection resulted in varicosities as well as the internalization of substance P receptors (SPR) within 5 min of stimulation. Both effects were reversible; within an hour varicosities and levels of internalized SP receptors returned to baseline values. Because the details of the studies by Mantyh et al. are important to the work we report here, we shall discuss these studies in more detail in the following paragraphs.

In the normal unstimulated spinal cord Mantyh et al. (1995a,b) found that distal dendrites of SPR-positive neurons varied little in diameter along their length (±1 μm over 20 μm) and that no neurons had more than five SPR-positive endosomes per cell body. After stimulation, 70% of SPR-positive cell bodies exhibited more than 20 endosomes. Five minutes after stimulation, the majority of SPR-positive distal dendrites appeared as a string of swollen varicosities (2–8 μm in diameter) connected by thin fibers with diameters 10–50% of those of the swollen varicosities. The varicosities contained 4–10 endosomes (0.1 and 0.7 μm diameter), whereas the thin fibers between them were virtually devoid of the endosomes (less than two per 10 μm of length).

After ligand binding, many receptors in the nervous system, especially the G-protein coupled receptors, undergo phosphorylation, endocytosis, and dissociation from the ligand in the endosome. Eventually such receptors are recy-

Received for publication 8 July 1996 and in final form 12 December 1996.

Address reprint requests to Dr. Darrell L. Tanelian, University of Texas Southwestern Medical Center, 5323 Harry Hines Blvd., Dallas, TX 75235-9068. Tel.: 214-648-5498; Fax: 214-648-2229.

0006-3495/97/03/1092/17 $2.00

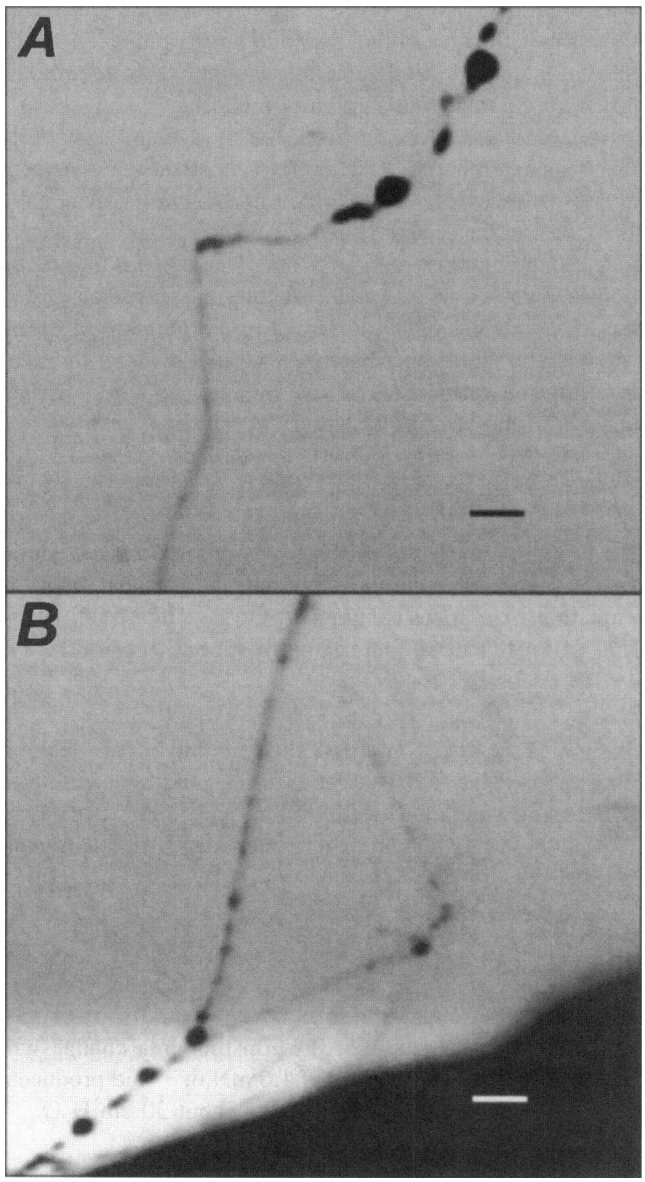

FIGURE 1 Epifluorescent photomicrographs of beaded nerve terminals from dorsal root ganglion neurons cocultured with epithelium. Beading was induced by the generation of shear stress to the neuronal membrane by a patch pipette. (*A*) Terminal branch of a neurite process, demonstrating irregular beading. (*B*) Regularly spaced spherical beading is more common than irregular beading. Also note in *B* that large beads are spaced further apart than small ones, and that small beads are usually interspersed between the large ones. The scale bars in each figure are 5 μm long.

cled back into the plasma membrane (Kobika, 1992). SP is released in the spinal cord upon noxious stimulation of innervated peripheral tissue (Duggan et al., 1991). SP is also known to excite spinal cord nociresponsive neurons (Salter and Henry, 1991) and to evoke a short-lived pain behavior (Wilcox, 1988). Mantyh et al. (1995a,b) hypothesized that somatosensory stimulation resulted in the release of SP, which subsequently binds with SP receptors, which were then internalized by endosome formations. This then resulted in the formation of varicosities through an as yet unspecified process. A schematic representation of this process is shown in Fig. 2.

Although SP receptor internalization occurred in all dendrites in which the SP receptor was occupied by the agonist, only the thin distal dendrites showed the structural reorganization. Mantyh et al. hypothesized that when a certain critical percentage of the plasma membrane is internalized together with the receptor, the dendrite undergoes structural reorganization, because the surface area decreases while the volume stays the same or increases. They felt that this effect would be relatively greater in small dendrites (Mantyh et al., 1995a,b). They also suggested that changes in the diameter and morphology of a dendrite should alter its passive electrical properties. Hence they hypothesized that the morphological reorganization of the distal dendrites might alter the integrative properties of the neurons and may constitute an important mechanism of neural plasticity.

A study employing patch-clamp recording at several sites on cultured DRG cells provided indirect evidence that varicosity formation may alter the transmission of action potentials (Wang et al., 1994). Whole-cell patch-clamp recordings were performed with electrodes located at either the DRG soma, a varicosity on a DRG neurite, or a DRG growth cone. Mean resting potentials recorded from varicosities were virtually identical to those obtained from

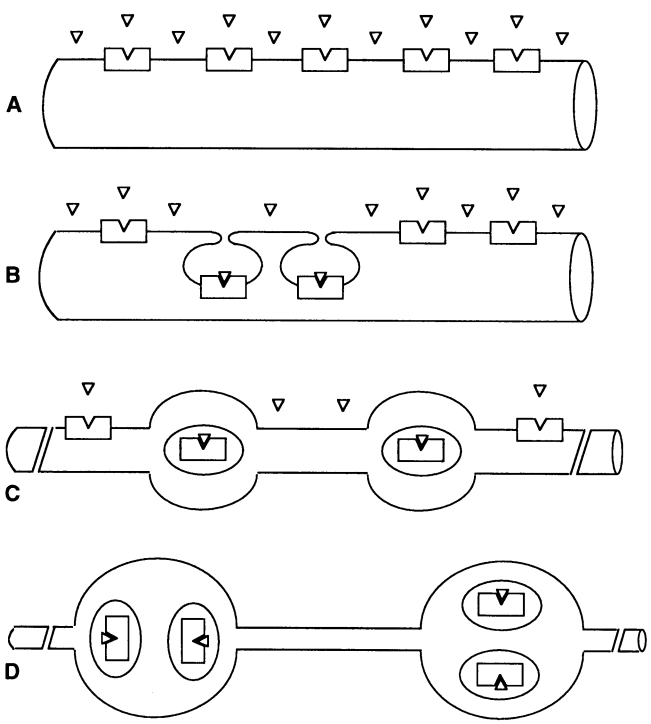

FIGURE 2 Schematic representation of receptor internalization and resultant dendritic transformation. (*A*) A terminal neuronal process with membrane receptors and unbound ligand. (*B*) As the ligand binds to its receptor, it initiates the process of receptor internalization by endosome formation. (*C*) After receptor internalization the cylindrical neural process becomes beaded. (*D*) A greater amount of receptor internalization leads to the formation of larger and further separated bead structures along the nerve fiber.

somas and growth cones (−56 mV versus 57 and 57 mV). However, depolarizing the membrane up to a +4-mV membrane potential failed to elicit action potentials from recording sites on varicosities, whereas action potentials were readily elicited from recording sites at the soma and growth cone. Furthermore, the mean membrane resistance recorded from varicosities was much less than that found at soma and growth cone sites (160 MΩ versus 687 and 922 MΩ). The authors hypothesized that perhaps varicosities blocked the transmission of action potentials, thereby promoting neurite outgrowth (which is inhibited by action potentials).

Because of the potentially great functional importance of these nerve fiber varicosities, we have set out to formulate a biophysical mathematical model of this phenomenon that is in agreement with known experimental data. The development of such a model is critical to understanding the functional implications of dendritic or axonal beading. It is virtually impossible to determine the electrical consequences of shape transformation in small nerve fibers (<4 μm radius) because of the difficulty and low success rate of accurately conducting electrophysiological studies on this fiber population. Using experimental data generated in our laboratory on DRG neurons in culture and the published data from the studies reported in the introduction, we have demonstrated that our biophysical models of shape transformation predict observed experimental data remarkably well. In addition, modeling of the resultant electrical fields generated by activation of these transformed processes has led to a quantitative functional understanding of how nerve fiber shape transformation can be used for information processing in the nervous system.

MECHANICAL ASPECTS OF BEADING

Dendritic shape transformation has been shown to be preceded by receptor internalization (Mantyh et al., 1995a,b). The chain of events that leads to the formation of a beaded structure may be either an active or passive process. At the present time, we cannot rule out an active process but will first consider the energetically more favorable possibility that shape transformation is a straightforward passive process. Receptor internalization along fine axonal or dendritic processes gives rise to mechanical forces of two origins. During internalization, a portion of the lipid bilayer together with the receptor is removed from the nerve fiber membrane to form an endosome, resulting in a reduction of its surface area. Because the volume of the nerve fiber remains the same or increases slightly, this creates membrane tension (membrane reduction model).

Another type of force is generated during receptor internalization because of the topology change that occurs when a membrane bilayer is transformed into a spherical endosome. In this process, the outer leaflet of the endosome membrane is derived from the inner leaflet of the plasma membrane and vice versa. Because of the small size of endosomes, there is a tangible difference in the area of their inner and outer lipid layers. This results in an unequal reduction in the area of the inner and outer lipid layers of the plasma membrane and generates spontaneous membrane curvature (spontaneous curvature model).

Both of these factors can cause thermodynamic instability of the plasma membrane. Therefore, to offset the generated stresses, the nerve fiber is forced to change its shape. We shall analyze the types of shape change that can result from both the membrane reduction and spontaneous curvature models. First we will estimate whether the forces generated due to membrane reduction will be enough to fluidize the cytoskeleton and redistribute the cytoplasm along the dendrite into the varicosities before engaging in a geometrical analysis of the beading process.

Forces and fluxes

If a cylindrical nerve fiber (Fig. 3 *A*) internalizes a fraction δ_A of its membrane and does not change its shape, then the remaining membrane is stretched by the same fraction δ_A. This will result in an increase in membrane tension:

$$\tau = \delta_A K, \tag{1}$$

where K is the area compressibility modulus. For a lecithin bilayer K is equal to 0.16 N m^{-1} (Evans and Skalak, 1980). The tension generated in the cylindrical nonbeaded nerve fiber with initial radius r_0 will then result in a pressure increase equal to

$$\Delta P = \frac{\delta_A K}{r_0}. \tag{2}$$

If the fractional change in area δ_A is about 1%, then in a nerve fiber with a radius of 0.5 μm this area change will generate a membrane tension of 1.6 mN m^{-1} and produce a pressure increase of 3 kPa, which is about 30 cm H_2O.

Is the cytoskeleton an obstacle to shape transformation?

Because of the presence of a cytoskeleton, the axoplasm of a nerve fiber is a rather rigid structure. To make the axo-

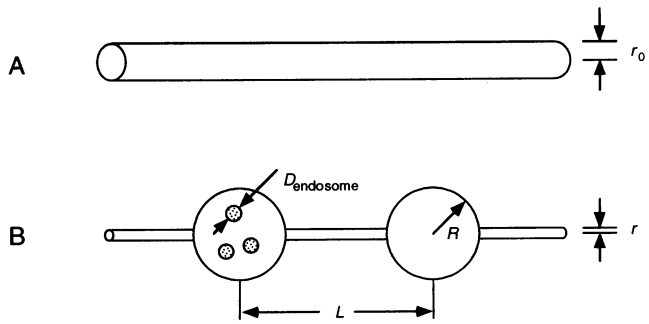

FIGURE 3 Schematic representation of idealized bead formation into regular spheres. The initial nerve fiber of radius r_0 is transformed into a beaded structure with spherical beads of radius R and connecting regions of radius r. The beads are filled with endosomes of diameter D and are separated by a distance L.

plasm flow, it is therefore essential to fluidize the cytoskeleton. The problem of cytoskeletal fluidization has been studied in a number of papers. Janmay et al. (1991) studied the reology of tubulin, actin, and vimentin, which are the basic structural elements of the major cytoskeletal components: microtubules, microfilaments, and intermediate filaments, respectively. They subjected microtubules, microfilaments, intermediate filaments, and fibrin to a range of shear stresses. The highest deformability was found in microtubule networks, which at the same time had the lowest fluidization threshold of 0.5 Pa, although Sato et al. found the value to be 1.4 Pa (Sato et al., 1988). F-actin is more resistant to deformation; it ruptures and begins to flow at a stress of 3.5 Pa. In contrast, fibrin and vimentin could be deformed to large strains under relatively high stresses and did not flow freely until a shear stress of 7 Pa was reached.

Estimation of the shear stress generated in a nerve fiber due to a decrease in membrane area will be compared to the amount required for fluidization of the various cytoskeletal components. If the pressure differential in a portion of a nerve fiber of length l is ΔP, then the total force pushing the cytoplasm out of a given cross section is

$$F = \pi r_0^2 \Delta P. \tag{3}$$

Before flow begins, this force is equilibrated by the shear force at the boundary between the cytoplasm and lipid membrane. The area of this boundary is

$$A = 2\pi r_0. \tag{4}$$

Therefore the shear force will be equal to

$$\sigma = \frac{F}{A} = \frac{r_0 \Delta P}{2l}. \tag{5}$$

As will be shown below, the average interbead period is about eight initial nerve fiber radii. Therefore, the shear force is about

$$\sigma = \frac{\Delta P}{8}. \tag{6}$$

Once the shear force becomes great enough the axoplasm will flow in both directions from the point of force generation. Then the cylindrical nerve fiber will transform into a beaded chain with interbead period L. Therefore, $l = L/2$.

Assuming the pressure, as we calculated before for a 0.5-μm-radius nerve fiber, is 3 kPa, the shear force generated in this fiber is 375 Pa. This value greatly exceeds the shear stress thresholds (σ_{th}) for fluidization of all structural cytoskeletal molecules.

Next it is important to estimate the time required to redistribute the cytoplasm into varicosities. The speed of this process will depend on the cytoplasmic viscosity. According to Poiseuille's law, if, in a cylindrical capillary of radius r_0, a pressure differential ΔP is maintained at a distance l, it should produce a flow of fluid with an average velocity

$$v_p = \frac{\Delta P r_0^2}{8\eta l}, \tag{7}$$

where η is the cytoplasmic viscosity. Because the pressure differential driving this process occurs over one-half of a beaded period ($l = L/2$), the characteristic time of cytoplasmic redistribution (t_{hyd}) can be estimated as

$$t_{hyd} = \frac{l}{v_p} = \frac{2\eta L^2}{\Delta P r_0^2}. \tag{8}$$

In our experiments, as well as in those of Mantyh, the average interbead period was equal to about eight initial nerve fiber diameters. Hence

$$t_{hyd} = \frac{128\eta}{\Delta P}. \tag{9}$$

Obviously this result depends on the cytoplasmic viscosity and on the pressure differential that was estimated earlier. The lower boundary for hydrodynamic time can be estimated by using the viscosity of water, $\eta_{water} = 1$ mPa · s. Then $t_{hyd} = 43$ μs. This is much faster than the data obtained experimentally.

Cytoplasmic viscosity has been measured in many cell types and is higher than that of water. For example, the cytoplasmic viscosity in fibroblasts has been shown to range from 1.1 to 1.4 mPa · s, whereas in the cytosol of sea urchin eggs it was measured to range from 2.1 to 2.5 mPa · s (Bicknese et al., 1993; Persiasami et al., 1991). In human neutrophils cytoplasmic viscosity is much higher and is pressure dependent (Tsai et al., 1993). It changes from 500 Pa · s at an aspiration pressure of 98 Pa to 50 Pa · s at 882 Pa. Applying these pressure-dependent viscosity numbers to our model, in which a 3-kPa pressure change is generated, results in a cytoplasmic viscosity in the range of 50 Pa · s. This number exceeds the viscosity of water by four orders of magnitude. However, even in this extreme case, where $\eta_{cytoplasm} = 50$ Pa · s, the redistribution of cytoplasm along a nerve fiber will take only 2.1 ms.

Nonideal initial shape considerations

The above calculations were done assuming the initial shape of the nerve fiber to be a circular cylinder and the beads to be perfect spheres. Actual nerve fibers are not perfect cylinders because the neuronal membrane is a somewhat flaccid tube. Therefore, our model gives only upper boundary values for forces, tensions, and pressures generated in a nerve fiber because of partial internalization of its membrane. Our estimate of shape transformation time, 2.1 ms, is therefore the fastest time in which this process could theoretically occur.

Because real nerve fibers deviate from perfect cylinders, the actual forces and tensions generated constitute only a fraction ($\epsilon < 1$) of the estimates given throughout the paper.

The cytoskeleton can be fluidized when a shear force given by Eqs. 2 and 9 exceeds the threshold σ_{th}. Taking into account the nonideal shape of the nerve fiber and the fact that only a fraction (ϵ) of the estimated pressure will actually be realized, one concludes that the shear stress rises according to the following equation:

$$\sigma = \frac{\varepsilon \delta_A K}{8 r_0}. \quad (10)$$

The result depends on the initial nerve fiber radius r_0, such that the smaller the fiber the larger the resultant shear force. Therefore one can expect that only nerve fibers smaller than a certain radius can attain the shear stress necessary to fluidize the cytoskeleton and transform a cylindrical process into a beaded one. In fact, it has been observed experimentally that dendrites larger than 2 μm in radius do not bead (Mantyh et al., 1995a,b). One can use this experimental value (2 μm) to estimate the shear stress threshold for cytoskeleton fluidization, and by knowing this value estimate the factor of nonideality ϵ. It has been shown experimentally that all cytoskeletal molecules can be fluidized by about 9 Pa of shear stress, whereas in an ideal 2-μm-radius neuronal process 94 Pa of shear stress can be achieved. Therefore the nonideality factor can be extimated to be ~0.1.

Cylindrical instability and pearling in long lipid tubes

The most obvious explanation for nerve fiber shape transformation is that the beading is caused by membrane tension generated because of receptor internalization. What are the consequences of this tension?

The problem of surface tension along a cylindrical body of fluid has interested people for a long time. It was known at the beginning of the last century that a cylinder of fluid is unstable and breaks into droplets to reach a state of minimum surface area. Another way for a cylinder to reduce its surface area without changing its volume is to undergo long-wavelength peristaltic deformation (Plateau, 1873). This situation holds true for any wavelength larger than the cylinder circumference. However, only a certain set of unique wavelengths are observed experimentally, even though energy considerations do not predict such a limitation. The dynamic nature of this phenomenon was investigated by Lord Rayleigh in 1892, who found the most unstable wavelengths (Lord Rayleigh, 1964).

Recently the problem of instability of cylindrical shapes resurfaced in connection with lipid membrane tubes, where a phenomenon very similar to beading along nerve fibers is observed (Bar-Ziv and Moses, 1994; Nelson et al., 1995). In these experiments, long cylindrical lipid bilayer vesicles were excited by laser tweezers with a spot size of 0.3 μm. The tubes were nearly straight cylinders with radii r_0 between 0.3 and 5 μm and a length of a few hundred microns, anchored at both ends by large globules of lipid. Application of the optical tweezers caused a dramatic transformation of the tube into a peristaltic shape. Once formed, the peristaltic shape had a well-defined wavelength (λ) with a normalized wave number $k = 2\pi r_0/\lambda$ between 0.64 and 1.00.

The shape change propagated in both directions from the point of laser application at a constant velocity between 10 and 70 μm s^{-1}. The membrane tension σ and viscosity of the intertube medium η determined the propagation velocity of shape transformation. Using dimensional analysis one can estimate the velocity to be

$$v_\sigma = \sigma/\eta. \quad (11)$$

Bar-Ziv and Moses (1994) estimated that to observe a propagation velocity of 30 μm s^{-1}, the tubes should be stressed to $\sigma = 2 \times 10^{-5}$ erg cm^{-2} $= 2 \times 10^{-5}$ mN m^{-1}. (This number is much lower than the stress estimate we made before for sensory dendrite receptor internalization.)

In the case of small tensions, a straight cylinder remains stable to all perturbations. For very high tensions, the model results in Rayleigh-type instability, such that pearling starts at normalized membrane tensions, $\sigma r_0^2/\kappa$, of about 6. Here κ is the bilayer bending stiffness. The stronger the laser tweezer force, the greater the generation of "membrane beads on a string" with interconnecting thin tubes (0.1–0.3 μm radius). Of interest is the observation that the beads travel along the tube toward the point of laser application and aggregate there. Their travel velocities are typically 0.1–10 μm s^{-1}. When traveling the beads are very spherical, and when they come to rest they become more flaccid. Removal of the laser energy allows newly developed beads to relax back to their initial straight cylindrical shape within 1 s, whereas the advanced beaded state can remain intact for many minutes.

The dynamic aspects of beading instability were analyzed theoretically by Nelson et al. (1995). They estimated that laser tweezers generate a membrane tension of about $\Sigma \approx 10^{-3}$ erg cm^{-2}, and that this value exceeds the critical value for shape transformation, $\Sigma_{crit} \approx \kappa/r_0 \approx 10^{-4}$ erg cm^{-2}. In this case, the tension was assumed to be distributed uniformly over the entire surface membrane; although, in fact, it propagates outward from the site of laser application. Their model also predicts that when the tension reverts to zero, the beaded tubule relaxes back to its initially stable cylindrical shape. Their conclusion was that membrane tension cannot destabilize the lipid membrane cylinder until the normalized wave number k exceeds 1, as observed experimentally.

Membrane reduction model

Suppose that the nerve fiber initially has a cylindrical shape with radius r_0 that transforms into a series of spheres and cylinders with radii R and r, respectively, and a period L (Fig. 3). The initial nerve fiber surface area and volume per period are then

$$A_0 = 2\pi r_0 L \quad \text{and} \quad V_0 = \pi r_0^2 L. \quad (12)$$

Now suppose a fraction δ_A of its membrane is internalized and equal to

$$A_{int} = 2\pi\delta_A r_0 L, \tag{13}$$

Then the surface area of the reshaped nerve fiber is reduced and becomes

$$A = 2\pi(1 - \delta_A)r_0 L. \tag{14}$$

Therefore, for the nerve fiber to remain cylindrical, its volume must decrease. However, its volume actually increases by the fractional amount δ_V, which is the volume of internalized endosomes, and results in a new final volume, equal to

$$V = \pi(1 + \delta_V)r_0^2 L. \tag{15}$$

After the shape transformation, the endosomes are found within the varicosities. If the average number of endosomes in a varicosity is n_{end} and their average diameter is D_{end}, then the internalized area and volume become

$$A_{int} = \pi n_{end} D_{end}^2 \quad \text{and} \quad V_{int} = \frac{\pi}{6} n_{end} D_{end}^3. \tag{16}$$

Comparing these formulas with Eqs. 13 and 15, one can find the fractional internalized area and volume:

$$\delta_A = \frac{n_{end} D_{end}^2}{2r_0 L} \quad \text{and} \quad \delta_V = \frac{n_{end} D_{end}^3}{6r_0^2 L}. \tag{17}$$

Therefore, after receptor internalization, the new area and the volume of one period of nerve fiber length become

$$A = 4\pi R^2 + 2\pi r(L - 2R), \tag{18}$$

$$V = \frac{4}{3}\pi R^3 + \pi r^2(L - 2R). \tag{19}$$

These new equations are related to the initial values in Eqs. 14 and 15 by the following equations:

$$4\pi R^2 + 2\pi r(L - 2R) = 2\pi r_0(1 - \delta_A)L, \tag{20}$$

$$\frac{4}{3}\pi R^3 + \pi r^2(L - 2R) = \pi r_0^2(1 + \delta_V)L. \tag{21}$$

This set of equations defines the relationship between the parameters of a beaded nerve fiber: L, R, and r. They are not a unique set of numbers, but rather are functionally interdependent, as represented by the curve in the three-dimensional plot (Fig. 4). This plot is graphed for the situation in which the fractional area of internalized membrane equals 0.01. This situation is very similar to the case of cylindrical instability analyzed by Lord Reyleigh, in which energy considerations also did not define a unique wavelength or even a unique band of wavelengths. The difference between the two cases is determined by the fact that the surface area of a nerve fiber is a constant, whereas that of a fluid cylinder is not. In living neurites, this parameter relationship is dynamic, and to determine the most likely parameter values

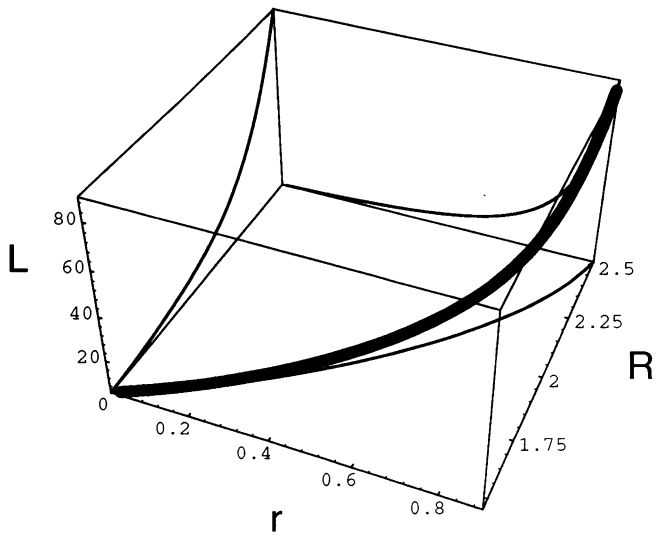

FIGURE 4 A three-dimensional plot describing the relationship between interbead period L, final bead radius R, and the connecting segment r. Note that the three variables are interdependent, as graphed by the heavy black line representing the possible combinations of the three variables.

at a given point in time it becomes necessary to place some limits on this model. Before doing so we will analyze this parameter relationship described by Eqs. 20 and 21 in more detail.

It is possible to eliminate one of the variables in these equations and express the radius of the varicosities R and their period L as a function of the radius of the connecting cylindrical segments r only:

$$R = \frac{(1 + \delta_V)r_0^2 - r^2 + \mathcal{A}}{(4/3)[(1 - \delta_A)r_o - r]}, \tag{22}$$

where

$$\mathcal{A} = \{[(1 + \delta_V)r_0^2 - r^2]^2 - 2.67 r_0 r[(1 - \delta_A)r_0 - r][(1 + \delta_V)r_0 - (1 - \delta_A)r]\}^{1/2},$$

$$L = \frac{2R(R - r)}{(1 - \delta_A)r_0 - r}. \tag{23}$$

These two functions actually define the projections of the three-dimensional curve onto the planes r–R and r–L, respectively. The dependence of R on r is presented in Fig. 5 *A* for different internalized areas. In practice, the internalized area is rather small and cannot exceed but a few percent. Therefore, the curves in Fig. 5 *A* are plotted with $\delta_A = 0.00$, 0.01, 0.05, and 0.10 (from the bottom to the top) and $\delta_V = 0$ everywhere. This simplification will be justified later.

In principle, the fiber radius (r) between the varicosities can change from 0 to $(1 - \delta_A)r_0$. As the upper limit of r/r_0 is approached, the curves become vertical (with the exception of the first curve, where $\delta_A = 0.00$). However, in practice, the most important values of r are the small ones.

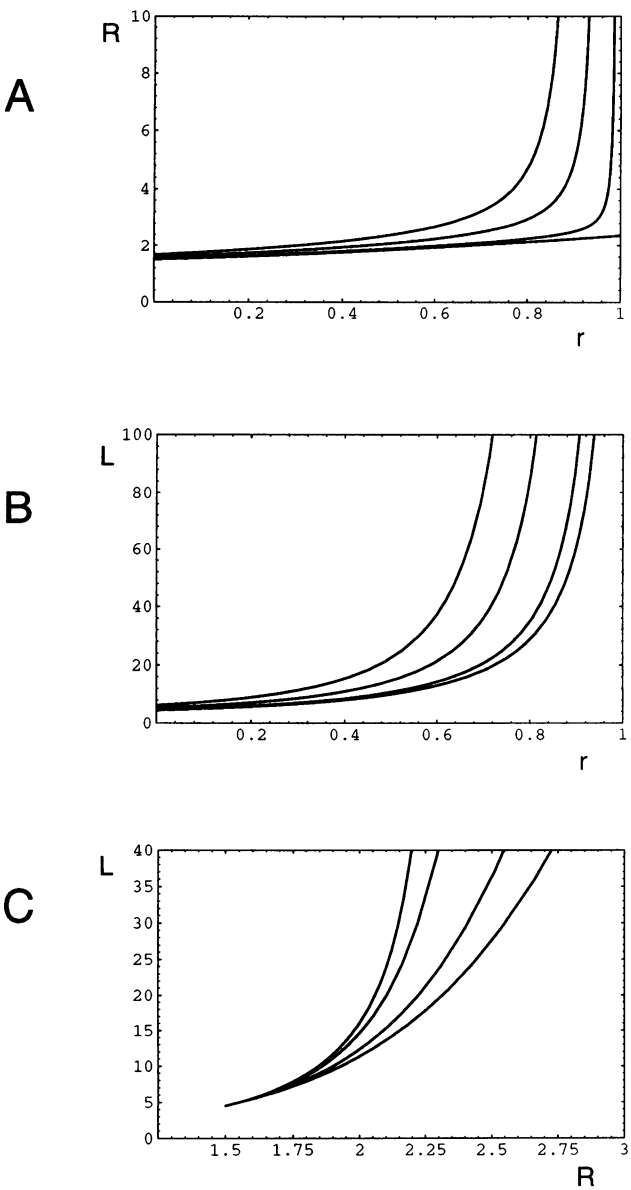

FIGURE 5 Families of curves for the transformation variables at different percentages of receptor internalization. (*A*) Final radius (R) versus connecting segment (r) plotted at increasing percentage receptor internalization. The leftmost curve represents 10% internalization, and each successive curve to the right represents 5, 1, and 0%, respectively. (*B*) Interbead period (L) versus connecting segment radius (r). The leftmost curve represents 10% internalization, and each successive curve to the right represents 5, 1, and 0%, respectively. (*C*) Interbead period (L) versus final bead radius (R). In this case the leftmost curve represents 0%, and as one moves to the right the percentage increases to 1, 5, and 10% internalization.

Over that range one can see that 1) the average radius of a varicosity R cannot be smaller than $1.5r_0$; 2) curves with different δ_A tend to merge; and 3) the curves are almost horizontal, i.e., the dependence of the size of varicosities on the radius r is very small. These results mean that one can predict the average radius of varicosities with a great deal of accuracy. For example, if $\delta_A = 0.02$, then for r in the range from 0 to 0.5 (this range covers all likely sizes of connecting fibers), the average radius of the varicosities changes from $1.53r_0$ to $1.93r_0$. Thus one can expect the mean value of varicosity radii (R_{mean}) to be about $1.7r_0$.

Fig. 5 *B* presents the relationship between the period of beading (L) and the radius of the connecting fibers (r) for the same set of internalized membrane fractions $\delta_A = 0.00$, 0.01, 0.05, and 0.10 (from the bottom to the top) and $\delta_V = 0$ everywhere. For the range of small r, the curves are very shallow, thereby allowing one the opportunity to accurately predict the average period. This period cannot drop below $4.5r_0$. If we select $\delta = 0.02$, the range for r from 0 to 0.5, then the average period (L) will vary from $4.78r_0$ to $11.51r_0$ with $L_{mean} = 8r_0$.

The relationship between L and R is presented in Fig. 5 *C* for the same set of δ values (from left to right). The curves merge in the beginning and then veer away from each other. It is worthwhile to note the relationship between the mean period and mean radius of varicosities:

$$L_{mean} = 4.7R_{mean}. \quad (24)$$

This estimate of the relationship between interbead period (L) and varicosity size (R) will be useful for the analysis of experimental data and in elucidating the mechanism of nerve fiber beading.

Spontaneous curvature model

Now let us consider how an uneven reduction of lipid molecules from two leaflets of nerve terminal membrane can influence its shape. This model was considered by Deuling and Helfrich (1977). Their studies were prompted by the observation that "myelin forms" sometimes evolve from red blood cells. These myelin forms are reminiscent of a regular string of beads. To explain this phenomenon, Helfrich and Deuling employed the concept of spontaneous or intrinsic membrane curvature. This concept states that a membrane has an intrinsic tendency to curve until it reaches a radius of curvature that requires no energy to maintain its shape. This radius is called the spontaneous radius of curvature. If the membrane is forced into another conformation, it develops tension and stores the work required as elastic energy. This energy is referred to as the elastic energy of curvature. Deuling and Helfrich, in their explanation of myelin forms, assumed that spontaneous curvature is constant over the total membrane, and their analysis predicted that a state of minimum energy can be achieved by the generation of a regular, almost sinusoidally varying varicosity along a string. This was in good agreement with experimental observation of myelin forms. If the size of the varicosities is very large, then their theory predicts a string of beads that are very closely apposed to each other. Unfortunately, this is not the case with our experiments.

Another approach to the problem of intrinsic curvature and shape transformation was developed by Markin et al. (1987b) in the analysis of osmotic shrinkage of giant lipid vesicles. The bending elastic energy of the bilayer is deter-

mined not simply by the geometric curvature, but rather by the difference between actual geometric curvature and spontaneous curvature. The change in shape from a cylinder to a beaded axon results in a change in axon membrane curvature and hence in a change in elastic energy. This certainly constitutes a contribution to the overall energy. This contribution comes primarily from bending of separate lipid monolayers. Besides that, there is another, more important contribution to the energy of elasticity. Because of the unequal removal of lipids from the inner and outer monolayers of the axonal membrane that occurs in the process of endosome internalization, one lipid monolayer becomes compressed in the lateral plane, and another becomes stretched. This assymetry is a major contribution to the elastic energy. However, this part of the elastic energy can be offset if the lipid monolayers are free to slide along each other and the membrane can change its shape. In ceratain cases the laterally mobile lipid monolayers can redistribute in such a way that this part in the elastic energy can be reduced to an absolute minimum (Markin et al., 1987b). This model is also referred to as the bilayer couple hypothesis (for a recent review see Seifert, 1994). We will now estimate this major contribution to the elastic energy.

In a curved membrane the difference in the radii of curvature is

$$r_{out} - r_{in} = h. \tag{25}$$

where h is about the thickness of one monolayer. The initial area of a nerve fiber is given by Eq. 12 in the previous section, and hence the difference in the areas of two monolayers is

$$\Delta A_0 = 2\pi Lh. \tag{26}$$

The total membrane area of all endosomes in one period of the string of beads is given by Eq. 16, and hence the difference between their outer and inner leaflets is

$$\Delta A_{end} = 4\pi n_{end} D_{end} h. \tag{27}$$

In the beaded nerve fiber this difference in area is added to the initial difference in leaflet area (Eq. 26), resulting in

$$\Delta A = 2\pi h(L + 2n_{end} D_{end}). \tag{28}$$

On the other hand, by knowing the shape of the beaded nerve fiber and its area (Eq. 18), one can easily find the difference between its two leaflets:

$$\Delta A = 8\pi Rh + 2\pi h(L - 2R). \tag{29}$$

Comparing this with Eq. 28, one finds

$$R = n_{end} D_{end}. \tag{30}$$

This result means that the nerve fiber can get rid of the major part of the elastic energy of curvature if the radius of varicosities after transformation reaches the value defined by Eq. 30. This is obviously an absolute minimum of this part of elastic energy, and the dendrite would naturally tend to seek a shape with these parameters. It is interesting to note that the optimum varicosity diameter (Eq. 30) is determined only by the size and the number of endosomes internalized within a given varicosity.

We have to mention here that flip-flop of lipid molecules between two monolayers can offset the difference in the area of two monolayers and eventually eliminate the reason for shape change. But the characteristic time of lipid flip-flop is many hours, whereas the effect we observed occurs in minutes and seconds. Therefore, even if in the long run flip-flop can change elastic energy and influence equilibrium distribution of lipids, it cannot have any impact on the phenomena developing in a course of seconds.

Reversal of nerve terminal beading

After termination of receptor internalization, a beaded dendrite can return to its original cylindrical shape. Because the reason for beading was a reduction of membrane area, its reversal should be based on an increase in membrane area per unit of neurite length. This can occur either by recycling of the endosome membrane back to the plasma membrane or by shortening of the fiber. In both cases the restraints that caused the beading would be relieved and the process can be reversed. However, in contrast to the original beading process, during reversal there is no active membrane force that can facilitate the reversal process. Therefore, reversal must depend upon intrinsic thermal energy or the repolymerization of cytoskeletal components. It then becomes reasonable to speculate that reversal of beading should take much more time than the initial beading process. This has been confirmed by experimental observations both in lipid bilayer tubes and in living sensory dendrites, where reversal of beading may take 30 min or more.

MATERIALS AND METHODS

Experiments were conducted on dorsal root ganglion (DRG) neurons in culture for 7–21 days. These experiments were designed to test our model of nerve terminal transformation by comparing the actual values obtained for r_o, R, and L in DRG nerve terminals (<2 μm radius) caused to bead by mechanical force or exposure to substance P with the values predicted by our geometrical model. These experiments were done not only to validate the geometrical model, but also to support the development of a theoretical model to explain the potential electrical consequences of beading.

Tissue culture preparation

DRG neurons were obtained and cultured with standard dissection and incubation techniques. Newborn Sprague-Dawley rat pups were anesthetized and decapitated, and their dorsal root ganglion was removed and placed immediately into chilled medium (Hanks' solution with 1 mg/ml collagenase). After dissection, trypsin (100–300 μl/ml) and DNase (0.5 mg/ml) were added to the medium and cells were incubated for 20 min with gentle agitation every 5 min. Cells were then centrifuged and washed twice with Hanks' solution. The Hanks' solution was then replaced with Dulbecco's minimum essential medium (DMEM) with 10% fetal bovine serum and triturated to separate cells. The cells were then washed again with DMEM + 10% fetal bovine serum and incubated for 1 h at 37°C and preplated twice to remove as many fibroblasts and Schwann cells as

possible. Cells were then counted, and 50 ng/ml of nerve growth factor (NGF) was added to the medium. The cells were plated in incubation medium composed of DMEM supplemented with penstrep (1%), N2 (Sigma I-1884, 5 μg/ml), bovine serum albumin (50 μg/ml), and NGF (50 ng/ml) at a final density of approximately 600 cells/dish in the center of 30-mm dishes that were precoated with Matrigel. Cells were thereafter incubated at 37°C.

Adenovirus containing the green fluorescent protein (GFP) construct alone (a gift from Dr. George Smith) was added to culture dishes (50 pfu/cell) 3 days after plating to identify the small-diameter nerve terminals of the DRG neurons. This fluorescent label allowed us to use epifluorescence and selectively visualize the fine nerve terminals before and after beading in culture among other supporting cell types.

Imaging

Neurons were visualized with a Nikon Diaphot 300 epifluorescent microscope fitted with Hoffman optics. The microscope was mounted on a *X-Y* platform controlled by a DCI 8000 position controller. This setup offered the ability to locate numerous neurons within a dish and store their *x-y* coordinates for repeat observation. Images were captured using a Hamamatsu C2400 High-Performance SIT camera. Image processing was achieved using MetaMorph (Universal Imaging Corporation) software. Neuronal processes were measured with calibration and measurement tools available in MetaMorph image analysis software.

Production of beading

Beading was produced in fine neuronal processes by the addition of 1 mM substance P (Sigma Chemical, St. Louis, MO) to the culture dishes under observation (Fig. 6). This high concentration was required because proteases in the culture medium can break down substance P. Other investigators, such as Patrick Mantyh, have used lower concentrations of substance P (1 μM) with the concurrent addition of protease inhibitors to elicit beading in DRG neurites in culture (personal communication). Beading was also produced by the application of mechanical force to the nerve terminal by a patch micropipette (Fig. 1). This experiment was done to verify studies in which high-energy mechanical stimulation produced varicosities in DRG processes (Suneson et al., 1989). In either case, beading is produced by the generation of membrane stress.

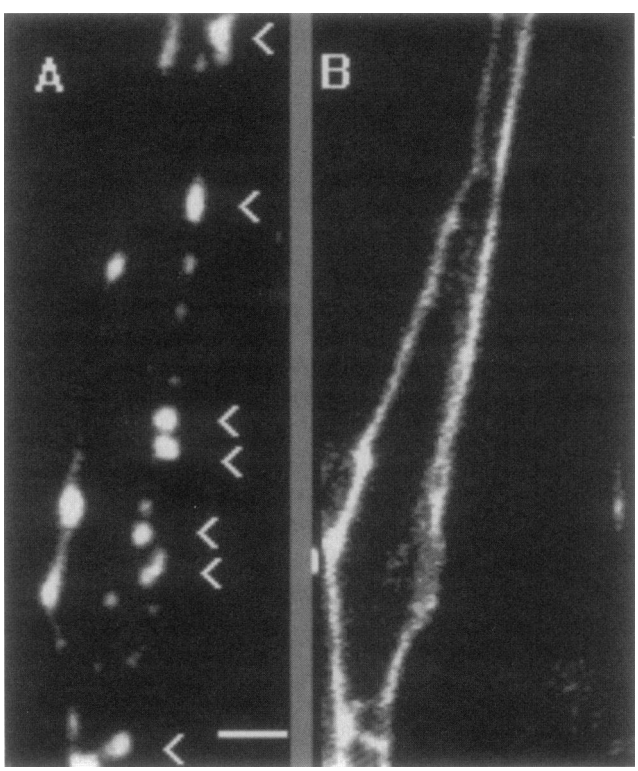

FIGURE 6 Epifluorescent photomicrographs of green fluorescent protein-labeled DRG neurons in culture before (*B*) and after (*A*) beading. The arrows mark the fiber and its associated beads, which were used for the calculations in Table 1 C.

RESULTS

The membrane reduction model of nerve fiber shape transformation predicts a rather narrow range of parameters for reshaped fibers. If the internalized area is only a few percent of the total surface area and the resultant connecting fibers are small in comparison with the original fiber diameter, then the average period L and radius of varicosities R are proportional to the initial dendrite radius r_0:

$$L = 8r_0 \quad \text{and} \quad R = 1.7r_0, \tag{31}$$

and they are related to each other by

$$L = 4.7R. \tag{32}$$

In rat spinal cord neurons, Mantyh et al. (1995a) observed transformation of dendrites when their initial radius (r_0) was less than 2 μm and found the resultant varicosity radius to range from 1 to 4 μm. They also observed from 4 to 10 endosomes per varicosity with diameters from 0.1 to 0.7 μm. Unfortunately, the authors (Mantyh et al., 1995a) did not give quantitative data for the periodicity of varicosities on transformed dendrites. However, inspection of figure 2 *D* in the paper by Mantyh et al. (1995a) reveals a string of five varicosities (four periods) with radii of about 4, 2.5, 2.5, 4, and 1 μm along a total distance of 60 μm. Therefore, this transformed dendrite displays an average varicosity period of 15 μm with an average varicosity radius of 2.8 μm (Table 1 A, experiment). From these measurements we can also estimate the internalized membrane area and volume change. The average number of observed endosomes was $n_{end} = 7$ and their average diameter $D_{end} = 0.4$ μm. If the initial dendrite radius was, say, $d_0 = 1.8$ μm, then one can

TABLE 1 Comparison of model predictions and experimental results

Data set		r_0 (μm)	L (μm)	R (μm)
Mantyh et al. (1995) (A)	Experiment	<2	15	2.80
	Geometrical model	1.8	14	2.95
DRG neurons in culture (B)	Experiment	0.6	5.6	1.08
	Geometrical model	0.6	4.8	1.02
DRG neurons in culture (C)	Experiment	1.1	9.0	1.92
	Geometrical model	1.1	8.8	1.87
DRG neurons in culture (D)	Experiment	0.4	3.0	0.65
	Geometrical model	0.4	3.2	0.68

find from Eq. 17 internalized fractions

$$\delta_A = 2\% \quad \text{and} \quad \delta_V = 0.15\%.$$

Therefore, the change in area with receptor internalization is much more pronounced than the change in volume.

The geometrical model we proposed is in relatively good agreement with the experimental data. For an initial dendrite radius of $r_0 = 1.8$ μm, our model predicts an average varicosity period of $L = 14$ μm and an average varicosity radius (R) of 2.95 μm (Table 1 A, geometrical model). Alternatively, using the curvature of elasticity model (Eq. 30), an average endosome number of 7, and an average diameter of 0.4 μm, this model predicts the final size of the varicosity (R) to be exactly 2.8 μm. Both of these models are in good agreement with the actual experimental data of Mantyh et al. (1995a) presented in Table 1 A (experiment).

In Figs. 1 and 6 we present experimental beading data from our laboratory conducted on dorsal root ganglion neurons in culture. In Fig. 1 *B* one can see a straight string of six varicosities with radii of 1.7, 0.6, 1.4, 1.0, 1.3 and 0.5 μm along a distance of 28 μm. Therefore, the average interbead period (L) is 5.6 μm, and the varicosity radius ranges from 0.5 to 1.7 μm, with an average value for R of 1.08 μm (Table 1 B, experiment). The initial neurite radius (r_o) was 0.6 μm. The geometrical model predicts a period of 4.8 μm and an average varicosity size (R) of 1.02 μm (Table 1 B, geometrical model).

In Fig. 6 one can see a string of seven varicosities with radii of 1.8, 1.9, 2.0, 2.0, 1.65, 2.0, and 2.1 μm. The average interbead period is 9 μm, and the average varicosity radius is 1.92 μm (Table 1 C, experiment). The initial neurite radius was 2.2 μm. Again, the geometrical model correctly predicts the average varicosity radius to be 1.87 μm and the average varicosity period (L) to be 8.8 μm (Table 1 C, geometrical). The data from Table 1 D come from a separate experiment whose figure is not presented in the text.

Both theoretical models, geometrical (membrane reduction) and membrane curvature, predict the initial and final dendritic varicosity parameters (r_0, R, L) with a high degree of accuracy as compared to actual experimental nerve fiber transformation data.

DISCUSSION

Nerve fiber shape and propagation of excitation

Changes in nerve fiber shape manifested by pronounced widening and/or thinning of their normally cylindrical shape (nerve fiber shape transformation) can change both active and passive neurite properties (Katz, 1966). Alteration of their electrotonic properties could have an impact on the integrative properties of the neuron. In addition, reshaping could influence the excitability of nerve fibers. These changes may lead to an increased probability of ephaptic transmission that could result in recruitment of additional dendritic or axonal processes as well as recurrent neural activation.

To analyze the ability of transformed nerve fibers to conduct nerve excitation, we can use the following analytical model of nerve impulse generation developed for squid axon (Markin et al., 1987a). In this model the sodium current was represented as a pulse of a current with a constant amplitude i_1 and time t_1, and the same for potassium current with a constant amplitude i_2 and time t_2. This model dramatically simplifies the analysis of nerve conduction in homogeneous and nonhomogeneous nerve fibers and neural networks, as well as ephaptic interaction between nerve fibers. For example, the velocity of nerve conduction is given by the following equation:

$$v = \sqrt{i_1/V_{th}R_{el}C^2}, \tag{33}$$

where V_{th} is a threshold of excitation and R_{el} and C are electrical resistance and membrane capacitance per unit length of the nerve fiber. The predictions of this equation are in good agreement with experimental observations. For example, for a squid axon with $i_1 = 63$ μA/cm, $t_1 = 0.35$ ms, $i_2 = 40$ μA/cm, $t_2 = 0.55$ ms, $C = 0.157$ μF/cm, $\rho = 50$ $\Omega \cdot$ cm (axoplasm resistivity), $d = 0.5$ mm (axon diameter), and $V_{th} = 18.5$ mV, this equation predicts $v = 23.4$ m/s, whereas the measured velocity is actually 21.2 m/s. A slight improvement of the theoretical equation, taking into account passive conductance of the axon membrane, improves the theoretical estimate to 21.5 m/s (Markin et al., 1987a).

It is easy to find from Eq. 33 the dependence of nerve conduction velocity on axon radius. Because $t_1 \propto r_0$, $R_{el} \propto r_0^{-2}$, and $C \propto r_0$, the resultant equation is

$$v \propto \sqrt{r_0}. \tag{34}$$

If the nerve fiber is electrically excitable, one can estimate its conduction velocity. If we assume that the electrical properties of the nerve fiber membrane are similar to those of the squid axon and it has a radius of $r_0 = 1$ μm, it follows from Eq. 34 that its conduction velocity should be $v_0 = 21.2\ (2/500)^{0.5} = 1.34$ m/s. Hence the length of the action potential rising phase along the original neuron is 470 μm.

After beading, action potential propagation along the nerve will change. The change in membrane area is insignificant (about 2%), and hence the current i_1 and capacitance C per unit length of the neuron do not change. However, the longitudinal resistance of the cytoplasm R_{el} will change dramatically and will be determined predominantly by the resistance of the narrowest axonal regions that connect the varicosities. As mentioned above, the dependence of resistance on radius is given by $R_{el} \propto r_0^{-2}$. Because the period L is related to the varicosity radius by equation $L = 4.7R$, the narrow fiber section represents only $12.7/4.7 = 0.57$ of the total nerve fiber length, and hence the conduction velocity of the beaded axon will be

$$v = \frac{v_0 r}{\sqrt{0.57 r_0}} = 1.3 v_0 \frac{r}{r_0}. \tag{35}$$

If the radius of the narrow connecting fiber decreases, for example 30 times, from 1 μm to about 34 nm, then conduction velocity will decrease to 0.058 m/s and the length of the action potential rising phase will decrease to 20 μm.

Equation 34, for conduction velocity, is applicable to a homogeneous fiber or to one in which the rising phase of the action potential covers many periods of beading. As illustrated by the previous example, the action potential length when reduced to only 20 μm relative to a beading period of 8 μm results in the action potential covering only two periods of nerve fiber beading. Under these conditions, action potential propagation along the beaded fiber can be blocked, and the limit of applicability of Eq. 34 is reached.

Action potential propagation along an axon with a single bead was studied by Jackson and Zhang (1995) in rat posterior pituitary nerve terminals. Their study was prompted by the fact that axons within the posterior pituitary contain many *en passant* swellings. The largest swellings observed along small-radius (0.2 μm) axons had radii up to 16 μm. The goal of their study was to determine the sensitivity of action potential propagation to this type of geometrical barrier and to small changes in membrane properties.

Experimental observations and numerical modeling by Jackson and Zhang (1995) provided the following axonal parameters: a resting potential of -67 mV, an action potential peak of 45 mV, a maximum rising slope of 218 V/s, a cytoplasm resistivity of 100 $\Omega \cdot$ cm, $d = 0.5$ μm, and a propagation velocity $v = 0.190$ m/s. To calculate the propagation velocity using Eq. 33 one needs to know the average activation current i_1, threshold potential V_{th}, and material parameters R_{el} and C. The last two are easy to calculate from the data given above. Analysis of the maximum rising action potential slope estimates the maximum activation current per unit area to be 218 μA cm^{-2}, with an average value of 109 μA cm^{-2}. The action potential threshold (V_{th}) was estimated to be 37 mV. These values and Eq. 33 estimate the action potential propagation velocity to be equal to 0.193 m/s, which is very close to the experimental observation of 0.190 m/s.

From these studies, Jackson and Zhang concluded that if membrane properties did not change in the process of swelling, action potentials propagate with high fidelity through a nerve terminal until the radius of the swelling exceeds 10 μm. Remembering that their original axon radius was 0.25 μm, this represents a ratio of 40:1, which is similar to our earlier calculation from Eq. 35, which predicts conduction block at a ratio of 30:1. The presence of additional axonal branches slightly decreases this critical size. The addition of an inhibitory GABAergic conductance localized to the varicosity membrane caused action potential failure at lesser bead radii. Therefore, the combination of geometrical barriers and altered membrane conductances can easily result in modification or block of action potential propagation. The specific size of the varicosity needed to block conduction is very dependent upon the unique properties of a given axon or dendrite and can vary over a rather broad range.

Impulse reflection

Nerve fiber shape transformation as described above can result in the creation of a neuronal reverberator with the potential for action potential generation or complete block of neuronal activity. After shape transformation, the fibers become nonhomogeneous and action potential conduction changes. If the difference between the radii of adjacent beads and connecting tubes is not large, the whole fiber can be described as a pseudocylinder and represented by average parameter values. Nerve conduction can also be considered to be pseudohomogeneous, with the spatial length of an action potential covering many periods of the beaded fiber. As the ratio of bead radius to connecting segment radius increases, action potential velocity decreases and the delay between excitations of neighboring beads increases. If this delay is comparable to the refractory period of the fiber, the excitation of a certain bead can result in electrotonic back-propagation of depolarization to the previous bead. This bead can then be reexcited and another action potential can propagate in the reverse direction.

What conditions are necessary for impulse reflection? When the nerve fiber radius changes, impulse conduction also changes in this region. It has been shown theoretically that when an impulse approaches a region of fiber widening, say from r to R, its velocity decreases, resulting in two different possibilities (Pastushenko and Markin, 1969). For small ratios of R/r, propagation continues into the larger radius region, even though action potential conduction is delayed. The reason for the delay is that the longitudinal current spreading from the action potential foot must suddenly excite a much larger membrane area. Propagation fails when R/r reaches a critical value. This value $(R/r)_{cr}$ depends on the specific membrane properties of a given fiber (Pastushenko and Markin, 1969; Khodorov 1974; Markin et al., 1987a). If the action potential has a safety factor of ~5, then a realistic estimate for $(R/r)_{cr}$ is ~4. The magnitude of action potential delay at the transition region between different fiber radii is very important, because if the delay is long enough, it can result in decremental reverse conduction (Khodorov et al., 1969).

In 1974 Goldstein and Rall considered this problem of impulse conduction through the point of nerve fiber broadening. They confirmed and critically analyzed the phenomenon of reverse conduction. In their specific example, when a critical value of 3.5 is reached, impulse conduction is blocked. For intermediate but subcritical values of R/r, e.g. 2.5, propagation may not only continue in the larger radius fiber, but can also reinvade the smaller fiber, developing a full-size impulse.

The phenomenon of action potential reflection has also been experimentally verified. Partial reflection of an antidromically propagating nerve impulse from the soma has been observed (Khodorov, 1974). Ramon et al. (1975) also observed partial action potential reflection in squid axons by using an internal axial wire to alter conduction properties along a segment of the nerve fiber.

Rinzel-Ermentrout model

An interesting theoretical analysis of nonuniform propagation along an excitable fiber was carried out by Rinzel and Ermentrout (1989). Instead of two homogeneous fibers in contact with each other, they considered a chain of excitable cells in which the coupling conductance between neighboring cells was identical. The last cell in the chain had a larger area than the other cells. The authors employed a two-variable model for excitable membranes formulated by Morris and Lecar (1981). In this model, an action potential is generated by an instantaneous voltage-gated inward calcium current and a delayed, voltage-gated, outward potassium current. These results fell in line with previous findings for a stepwise change in a nerve fiber radius. An action potential could easily propagate along the chain from one cell to another. However, if the last cell was larger than the others, the impulse could not excite it. In their model, conduction block was found along the chain when the area ratio reached 10 (ratio of radii 3.16), whereas conduction delay and reflection were found for an area ratio of 6.25 (radii ratio 2.5). This example may also be relevant to the behavior of a beaded dendrite.

Passive electrical properties of the chain of spherical cells in the Rinzel-Ermentrout model are very similar to the properties of a beaded nerve fiber with narrow connecting tubes. If we adopt the same excitability model for the beaded nerve fiber, we can anticipate that a number of important phenomena will occur.

Reverberator

If all beads along a nerve fiber have the same size, the action potential can propagate along this chain unless the coupling conductance becomes too small (i.e., the ratio of bead radius to connecting segment radius is large). In reality, the beading process is always random and results in a statistical distribution of beads. Therefore, one can always find large and small beads interspersed among each other. As we found in the previous example, if the ratio of adjacent bead radius to connecting segment radius is about 2.5, this bead can both allow passage of an impulse as well as generate another one in the retrograde direction.

If there are two large beads in a string separated by one or more smaller beads, as in Fig. 7, this group may become a reverberator or a generator of impulses. In the absence of external excitation, this set of beads exists in a resting state. When an action potential arrives from outside of this beaded region, it initiates reentrant activity inside the reverberator (Fig. 7). In this figure, the initial impulse (AP_{init}) arrives at the first large bead, where it splits into two impulses, AP_2 and Ap_3. Impulse 3 propagates inside the generator and reaches the second large bead, and again two impulses are generated: one returns to the generator and the other propagates away from the generator. Impulse 2 is reflected and propagates in a retrograde direction.

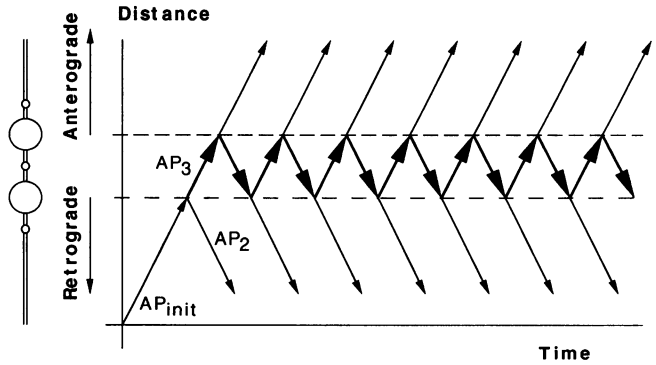

FIGURE 7 A pair of reflecting beads along a nerve fiber. In this case a single action potential (AP_{init}) entering a region of two reflecting beads (a reverberator) can produce recurrent generation of both anteriograde and retrograde nerve impulses. The resultant frequency is the intrinsic frequency of the reverberator. Thus a single action potential can be multiplied many times before reaching its destination.

As a result, one impulse always remains trapped in the generator and reflects between its ends. Every time this entrapped impulse reflects from the beaded ends it sends impulses in both anterograde and retrograde directions along the nerve fiber. Therefore, the beaded fiber can maintain its activity indefinitely, or until further changes in neuron activity provide a block of impulse propagation, or mechanical relaxation occurs and the beaded nerve terminal reverts to its original cylindrical shape.

Interestingly, this permanent reentrant activity can be triggered by a single external impulse. Emerging activity is periodic, with the period determined by the size of the reverberator and the propagation velocity.

Frequency modulation

Suppose that an external source generates a train of impulses with frequency f_{in}, and this train runs into a single reflecting bead (Fig. 8). In this case, every second impulse will be annihilated by collision with reflected impulses. Hence the frequency of the train that passes through the reflecting bead will decrease by half, becoming $f_{out} = f_{in}/2$.

Now suppose that a nerve fiber has two reflecting beads, which comprise a reverberator with an intrinsic frequency f_{rev}. If a train of impulses with frequency f_{in} enters this fiber (Fig. 9), then at the exit it will have a frequency f_{out} given by the following equation:

$$f_{out} = \begin{cases} f_{rev}, & \text{if } f_{in} \le f_{rev}; \\ \dfrac{f_{in}}{1 + [3/Q(f_{in}/(f_{in} - f_{rev}))]}, & \text{if } f_{in} > f_{rev}, \end{cases} \quad (36)$$

where $Q(x)$ is an integer part of x, i.e., the largest integer not exceeding x.

The plot of f_{out} versus f_{in} is presented in Fig. 10 *A* by a solid line. Both frequencies are normalized by the intrinsic frequency of the reverberator f_{rev}. In the absence of a reverberator, the train of impulses would not be altered, and

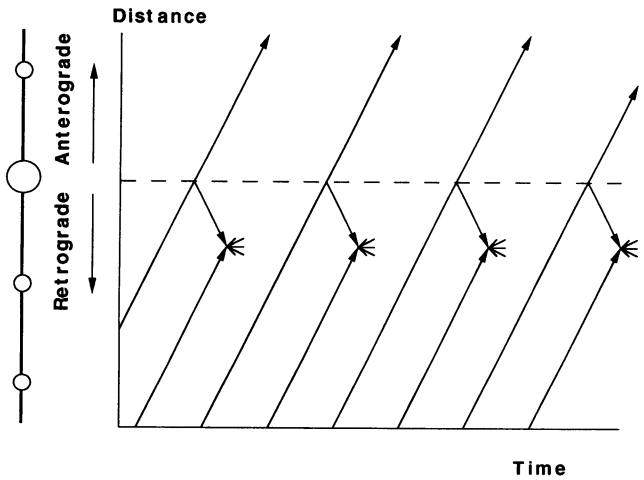

FIGURE 8 A single reflecting bead along a nerve fiber. This condition can transform an action potential train of input frequency f such that the output frequency equals $f/2$. Note that when an incoming action potential collides with a reflected retrograde impulse, the two are annihilated.

f_{out} would equal f_{in}. This reference case is represented in the figure by the broken line with a slope of 1. In the presence of the reverberator, the train of impulses undergoes a frequency transformation. There are three characteristic transformation regions: low frequency (I), where $f_{in} \leq f_{rev}$; intermediate frequency (II), where $f_{rev} < f_{in} \leq 2f_{rev}$; and high frequency (III), where $f_{in} > 2f_{rev}$. In the first region, f_{in} is augmented to a constant level equivalent to the intrinsic reverberator frequency f_{rev}. If the frequency f_{in} exceeds the frequency of the reverberator f_{rev}, the input is filtered. This process is easy to understand in the case of high-frequency input, where $f_{in} > 2f_{rev}$. At each reflecting bead the number of impulses in the train is reduced by one-half. This means

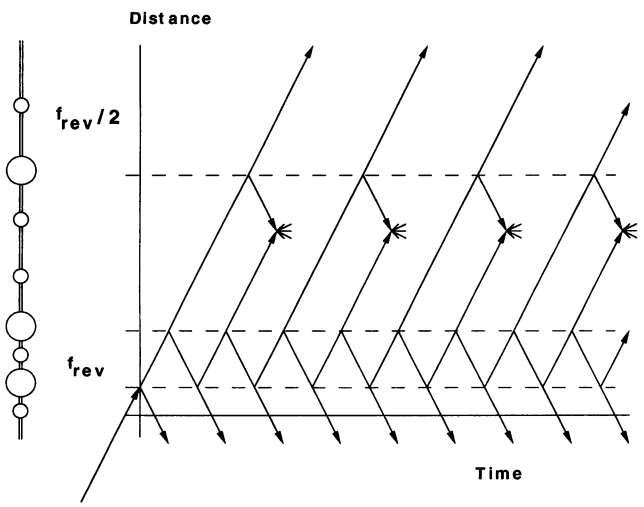

FIGURE 9 A single reverberator and one reflecting bead. In this case, note that when a single action potential enters the first pair of beads (reverberator), it emerges with an intrinsic frequency, f_{rev}. In this case the single reflecting bead transforms the emergent reverberator frequency (f_{rev}) such that the final output frequency becomes $f_{rev}/2$.

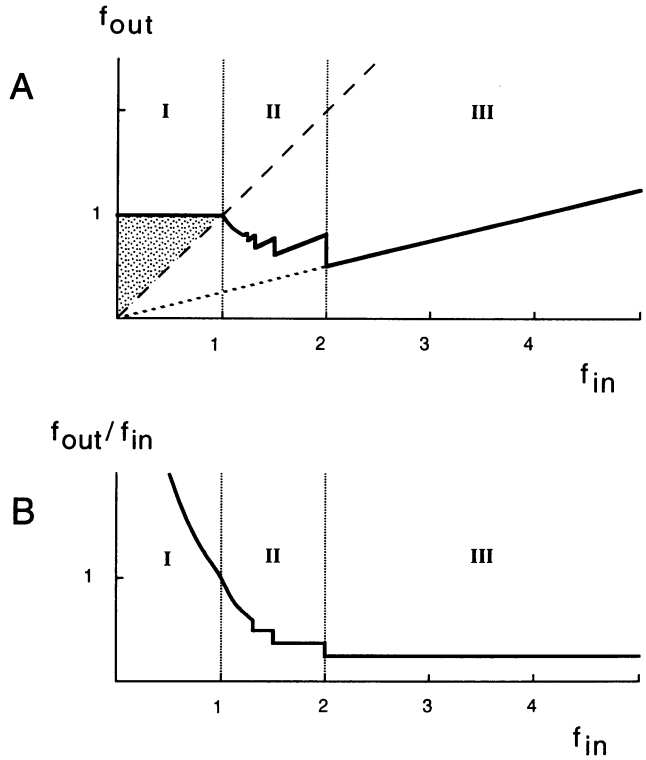

FIGURE 10 Frequency transformation in a beaded nerve fiber. (*A*) A plot of the relative output frequency as a function of input frequency for a beaded nerve fiber. The broken line represents a normal cylindrical nerve fiber where input equals output. Note that when $f_{in} < f_{rev}$ (region I) that the input frequency is amplified such that $f_{out} = f_{rev}$. For the case in which $f_{rev} < f_{in} < 2f_{rev}$ (region II), the output frequency decreases nonlinearly. When $f_{in} > 2f_{rev}$ (region III), then f_{in} is linearly reduced by a fraction of 1/4. (*B*) A plot of the transformation coefficient versus input frequency f_{in}. Again, when $f_{in} < f_{rev}$, the coefficient is >1, indicating amplification. Between $f_{rev} \rightarrow 2f_{rev}$, the input frequency is nonlinerally filtered and has a value between 1 and 0.25. When $f_{in} > 2f_{rev}$, the coefficient becomes linear at a value of 0.25.

that at the exit only one-fourth of the initial impulses are preserved. In other words, the frequency is reduced by a factor of 4 and the slope of the line in the corresponding region of Fig. 10 *A* III is 1/4. In this region the filtering is linear. The intermediate region displays nonlinear impulse reduction due to the integer nature of the filtering process. Therefore, the three characteristic regions presented in Fig. 10 can be referred to as regions of amplification, nonlinear filtering, and linear filtering, respectively. It is interesting to note that in the intermediate region of nonlinear filtering the output frequency is not increasing with the input frequncy, but rather is decreasing.

Another useful parameter for describing this process is the transduction coefficient $\alpha = f_{out}/f_{in}$. In a uniform fiber the transduction coefficient is constant: $\alpha = 1$. In a fiber with a single bead it is also constant, but smaller: $\alpha = 1/2$. In a fiber with a reverberator, the transduction coefficient is frequency dependent, as presented in Fig. 10 *B*.

In the case of a series of N beads along a nerve fiber, if the input frequency is high enough, then after each reflect-

ing bead the frequency of the train will be decreased by one-half, such that

$$f_{out} = 2^{-N} f_{in}.$$

If the length of the string is L_{chain} and the average period, as before, is designated L, then this equation can be rewritten as

$$f_{out} = 2^{-L_{chain}/L} f_{in}.$$

Hence, if the beads have a uniform period, then there is an exponential attenuation of the input frequency along the chain of beads. If the beads are aperiodically distributed, then the frequency attenuation deviates from a perfectly exponential decay.

In Fig. 11 we depict the four cases of frequency modulation that can occur along a beaded dendritic chain. As shown in case 4, this equation holds true only if the input frequency is higher than the highest intrinsic reverberator frequency along the beaded chain. An estimate of this limiting frequency is

$$f_{lim} = f_{rev}/2^N.$$

If this is not the case, then the train of impulses will disappear along the beaded chain and the frequency will become equal to the average intrinsic frequncy of the beaded chain (Fig. 11, cases 3 and 2). Moreover, if the input frequency is below the intrisic frequency of the beaded chain, then the input will be amplified to a stable output frequency equal to the intrinsic frequency (Fig. 11, case 1).

This analysis can also be applied to the interaction of multiple reverberators. Suppose we have two reverberators with frequencies $f_1 > f_2$. The intrinsic frequency of a reverberator depends on the length of the reverberant pathway: the longer the distance, the lower the frequency. Impulses emitted by these reverberators will collide somewhere in the region between them (Fig. 12). If the two reverberators have the same frequency, consecutive impulses will always collide at the same location. However, if one reverberator generates impulses faster than the other, its exiting impulses will encroach upon the slower reverberator and eventually invade it. The following events are rather interesting.

This impulse invasion will terminate activity in the slower reverberator because the invading impulse will collide with the internal action potential of the second reverberator and annihilate it. Thus the slower reverberator will be shut down, while the faster one will continue its activity. However, upon reaching the slower reverberator, an impulse is reflected back toward the faster reverberator and will annihilate the next approaching impulse. Only the second impulse will be able to reach the slower reverberator and reactivate it. Then it will be shut down again and reactivated.

Therefore, the total activity of a neuron with two reverberators with frequencies f_1 and f_2 is determined by the fastest one (f_1). The faster reverberator becomes a pacemaker and synchronizes the activity of the other one with its own. It is interesting to note that the frequency of the second reverberator becomes completely determined by the first one. In a branching beaded nerve fiber additional possibilities for impulse interaction exist.

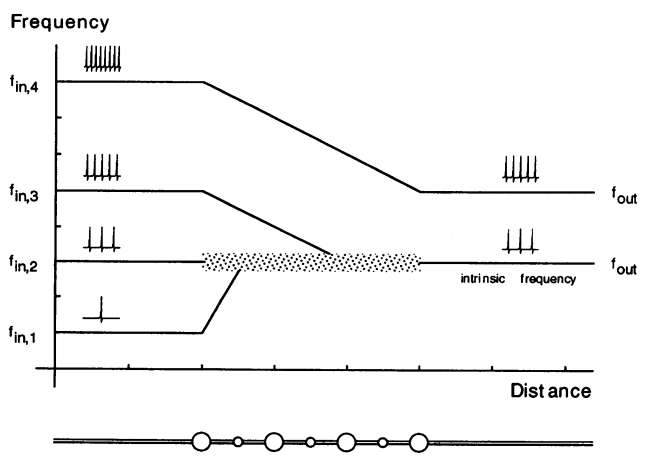

FIGURE 11 A schematic representation of what occurs along the length of a beaded nerve fiber. Note that the stippled region is a schematic representation of the beaded nerve fiber region. There are four cases to be considered: 1) $f_{in,1}$, where the input frequency is less than the intrinsic frequency and the signal is amplified to where $f_{out} = f_{intrinsic}$; 2) $f_{in,2}$, where the input frequency equals the intrinsic frequency and $f_{in,2}$ equals f_{out}; 3) $f_{in,3}$, where the input frequency is greater than the intrinsic frequency, but nonetheless, $f_{out} = f_{intrinsic}$; and 4) $f_{in,4}$, where the input frequency is $> 2^N f_{intrinsic}$ and the resultant f_{out} is greater than the intrinsic frequency.

Ephaptic cross-excitation of nerve fibers

Beaded neuronal processes constitute an interesting system capable of modifying incoming electrical information. As we have discussed, there are a number of possible theoretical and functional consequences of dendritic or axonal beading. Moreover, there is the additional possibility that

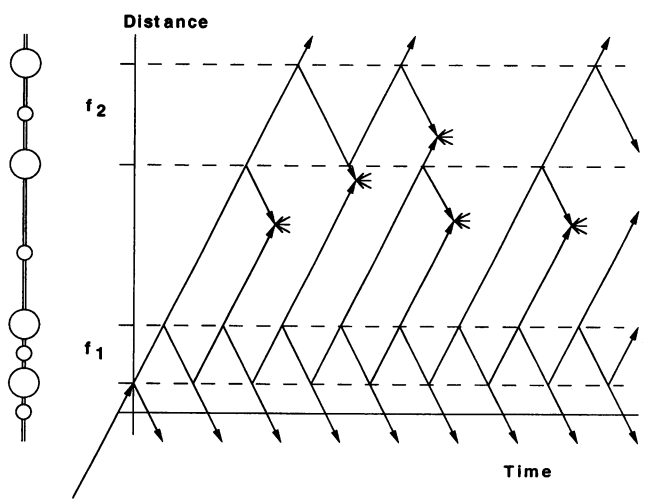

FIGURE 12 Two reverberators in series. Note that the reverberator f_1 with the higher intrinsic frequency becomes the impulse generator and that the slower reverberator f_2 modifies the final neural output.

interfiber cross-excitation of adjacent nerve fiber beads can occur. Early studies of electrical interaction between nerve fibers done by Katz and Schmitt in 1940 found that an impulse traveling in one fiber changes the excitability of the second fiber. They also studied simultaneous passage of impulses in two fibers. Under certain conditions they observed that two parallel fibers with different initial conduction velocities interact in such a way as to produce a collective impulse that synchronizes the individual action potentials, making their conduction velocities equal. When the initial action potential velocities are equal, the resultant impulse velocity becomes slower. The fiber interaction depends greatly on the resistance of the surrounding medium, such that cointeraction of fibers increases with increasing extracellular resistance. This phenomenon makes axonal cross-excitation possible only if extracellular resistance is very high (Markin et al., 1987a). Therefore, it is practically impossible to have cross-excitation between two adjacent cylindrical nerve fibers with equal excitation thresholds.

Cross-excitation becomes much more favorable in a nerve bundle consisting of many nerve fibers (Markin et al., 1987a), where simultaneous activation of many nerve fibers can produce an aggregate current that can activate the nonactive fibers in the bundle. Cross-excitation is also greatly facilitated by inhomogeneity of nerve fibers, beading being a prime example of this type of inhomogeneity. The production of reverberators in beaded fibers leads to regenerative action potential activity, which could lower the excitability threshold of the nerve due to recurrent depolarization and accumulation of potassium in the extracellular space after prolonged neuronal activity. Therefore, under the right circumstances it may become possible to cross-excite dendritic adjacent axonal and or dendritic processes.

Functional implications of nerve fiber beading and resultant frequency modulation

The model presented in this paper is very intriguing because its predictions are in good agreement with a number of unexplained electrophysiological and psychophysical phenomenon known to be mediated by small-diameter neuronal processes. In the somatosensory system it has been demonstrated that both amplification and activity-dependent depression of mechanosensory nociceptors can occur, but no single fundamental mechanism has been suggested to explain these phenomena (Clatworthy and Walters, 1993a,b). Clatworthy and Walters (1993b) demonstrated electrophysiologically that when an electrical stimulus (0.5-s DC shocks) first activates peripheral mechanoreceptors, resulting in the generation of <6 action potentials per shock (shock, low activation; Fig. 13), each subsequent stimulus of equal magnitude generates progressively more action potentials per shock over the next three shocks, until spike generation per shock plateaus at about 160% of the original stimulus-evoked spike number (Clatworthy and Walters, 1993b). This phenomenon is an example of sensory amplification occurring when the original spike input is low and is comparable to the theoretical model prediction depicted in Figs. 10 and 11, $f_{in,1}$, where an initial low spike input gradually produces beading, which then results in progressive amplification of action potential number until the input frequency reaches the intrinsic frequency of the beaded axon and the output frequency plateaus.

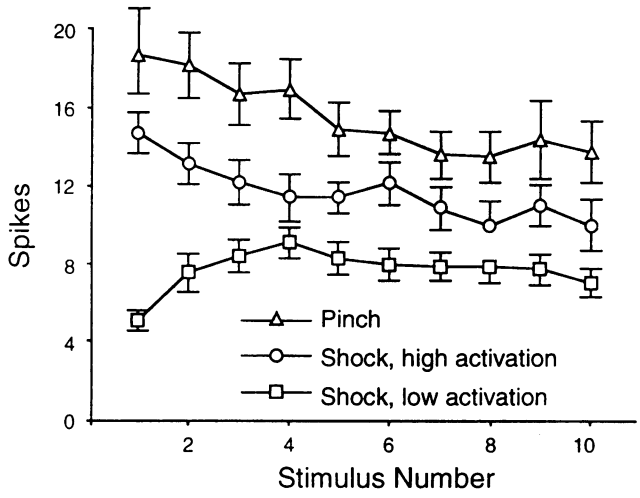

FIGURE 13 This is a duplication of figure 3 from Clatworthy and Walters (1993b). This figure shows amplification and depression of sensory responses (spikes) occurring after multiple stimulus trials. The mean number of spikes (mean ± SE) is plotted for cells whose receptive fields on the tail of *Aplysia* were stimulated 10 times, at 5-s intervals, with either shock (2–10 ma) or forceps pinch, each of 0.5 s duration. Single, 0.5-s DC shocks were delivered through a long subcutaneous electrode implanted in the dorsal surface of the tail. Cells are divided into three groups on the basis of their initial discharge to stimulation: cells initially responding with >12 spikes (shock, high activation (n = 7) and pinch (n = 23)) and cells showing a low initial response of <6 spikes (shock, low activation; n = 25).

In contrast, when the initial spike number per stimulus is large (>14) because of electrical (shock, high activation; Fig. 13) or mechanical (pinch; Fig. 13) stimulation, each subsequent stimulus produces progressively less action potential until the spike number again plateaus at a value that is ~70% of the initial stimulus-evoked spike number (Fig. 13, shock, high activation and pinch) (Clatworthy and Walters, 1993b). This phenomenon is called activity-dependent depression of mechanosensory discharge. Our theoretical model predicts that a high-frequency initial spike input would cause rapid beading and, as depicted in Fig. 11 ($f_{in,3}$), reduce subsequent stimulus-evoked spike output. In both experimental cases (Fig. 13), initially high (shock, high activation; pinch) or low (shock, low activation) initial spike number becomes comparable after multiple stimulus trials and could be considered equivalent to the intrinsic frequency of the dendritic transformation model. Another prediction of the beading model is that the overall action potential conduction velocity along a beaded process should be slowed. The experimental studies of mechanonociceptors found that after repeated stimulation, either electrical or mechanical, action potential conduction was slowed by 12% and 6%, respectively.

The observation that sensory amplification or depression occurs is not limited to the above set of electrophysiological studies, but has been shown in numerous electrophysiological and psychophysical studies (Beitel and Dubner, 1976a,b; LaMotte et al., 1984; Perl, 1968). In monkey C polymodal nociceptors, Beitel and Dubner demonstrate that repeated noxious thermal stimulation can initially produce enhanced action potential generation on repeat stimulation and that subsequent stimulation will eventually result in a depressed response and even complete cessation of neural activity, despite maintenance of the stimulus. These findings are consistent with our model in that it predicts that 1) initially a noxious stimulus should cause receptor internalization and beading in small-diameter axons or dendrites and amplify activity; 2) repeat or prolonged activity should increase the bead-to-connecting stalk diameter and thereby depress or filter the neural activity; and 3) if sufficient prolonged activation occurs, then the bead-to-connecting segment diameter can become great enough to block action potential conduction. It is often reported clinically that after sudden massive tissue injury, patients experience no pain for periods up to several hours later. A further prediction of this model is that once beading has occurred, it should result in an afterdischarge after stimulus removal (Fig. 7), and this is consistent with the response characteristics of polymodal nociceptors after noxious thermal stimulation (Beitel and Dubner, 1976a,b).

Human C fiber nociceptors demonstrate an interesting phenomenon, in that after an initial noxious thermal stimulus, the action potential output rapidly adapts during a maintained, constant-magnitude stimulus (LaMotte et al., 1984). However, the subsequent stimulus does not result in attenuation of the neural output, but rather neural activity remains constant throughout the duration of the stimulus (LaMotte et al., 1984). In both the human electrophysiology and psychophysical experiments, neural activity and sensation outlasted stimulus duration (LaMotte et al., 1984). The plateau of neural activity and poststimulus response on repeat stimulation can be explained by initial stimulation-induced beading producing an intrinsic, regenerative, action potential frequency within the involved sensory fiber. There are many clinical examples of both posttraumatic sensitization (hyperalgesia) and pain persisting beyond the removal of a stimulus (hyperpathia).

The functional consequences of beading should not only apply to the transient varicosities formed by receptor internalization, but also to longer-lasting varicosities containing new presynaptic terminals that are formed during the acquisition of some kinds of long-term memory (Bailey and Kandel, 1993). Under appropriate conditions, new, *en passant* synaptic varicosities might give rise to reverberation that could significantly amplify activity triggered in a neuron that had been transformed by learning, and thus contribute to the readout of memory. Although this possibility has not yet been tested directly, a suggestive parallel exists between increased varicosity number and increased probability of afterdischarge in sensory neurons of *Aplysia*. Training this animal with repeated noxious stimuli causes a long-term (up to weeks) increase in both the number of varicosities (Bailey and Chen, 1988; Nazif et al., 1991) and incidence of afterdischarge triggered by brief intracellular stimulation of sensory neurons (Walters, 1987).

It becomes readily apparent that by varying the size and distance between the dendritic beads, infinite possibilities exist for modifying neural input after dendritic transformation. The transformed dendrites or axon terminals can result in any or all of the following transformations of the original or subsequent neural impulses: amplification, filtering, continuous ectopic impulse generation, or complete neural blockade. These modifications may have relevance for the generation of pain states (primary or secondary hyperalgesia, hyperpathia, ectopic nociceptive impulse generation), cardiac arrythmagenicity, muscle spasms, seizures, and hallucinations. In addition, nerve fiber transformation may be involved in the mechanism of counter-irritation-induced analgesia such as occurs with massage, vibration, electrical stimulation (TENS, PENS, peripheral nerve, spinal cord and deep brain stimulation) and other forms of stimulation-induced analgesia.

We wish to thank Professor Edgar T. Walters for allowing us permission to publish figure 3 from his paper (Clatworthy and Walters, 1993b) as Fig. 11 in our text. We also greatly appreciate his helpful discussion of his sensory physiology research.

This work was supported by the Sid W. Richardson Foundation and the Jane and Bill Browning, Jr., Chair in Medical Science, held by D. L. Tanelian.

REFERENCES

Anderson, P. L., and J. R. Bamburg. 1981. Effect of local anesthetics on nerve growth in culture. *Dev. Neurosci.* 4:273–290.

Bailey, C. H., and M. Chen. 1988. Long-term memory in *Aplysia* modulates the total number of varicosities of single identified sensory neurons. *Proc. Natl. Acad. Sci. USA.* 85:2373–2377.

Bailey, C. H., and E. R. Kandel. 1993. Structural changes accompanying memory storage. *Annu. Rev. Physiol.* 55:397–426.

Bar-Ziv, R., and E. Moses. 1994. Instability and "pearling" states produced in tubular membranes by competition of curvature and tension. *Phys. Rev. Let.* 73:1392–1395.

Beitel, R. E., and R. Dubner. 1976a. Response of unmyelinated (C) polymodal nociceptors to thermal stimuli applied to monkey's face. *Brain Res.* 112:402–406.

Beitel, R. E., and R. Dubner. 1976b. Fatigue and adaptation in unmyelinated (C) polymodal nociceptors to mechanical and thermal stimuli applied to the monkey's face. *J. Neurophysiol.* 39:1160–1175.

Bicknese, S., N. Periasami, S. B. Shohet, and A. S. Verkman. 1993. Cytoplasmic velocity near the cell plasma membrane: measurement by evanescent field frequency-domain microfluorimetry. *Biophys. J.* 65: 1272–1282.

Bird, M. M. 1978. Microsurgical transection of small nerve fibre bundles in vitro. Effects of axons, growth cones and glial cells. *Cell Tissue Res.* 190:525–538.

Cajal, S. R. 1952. Histologie du System Nerveux de l'Homme et des Vertebres, Vol. 1. Instituto Ramon Y. Cajal, Madrid.

Cajal, S. R. 1955. Histologie du System Nerveux de l'Homme et des Vertebres, Vol. 2. Instituto Ramon Y. Cajal, Madrid.

Clatworthy, A. L., and E. T. Walters. 1993a. Rapid amplification and facilitation of mechanosensory discharge in *Aplysia* by noxious stimulation. *J. Neurophysiol.* 70:1181–1194.

Clatworthy, A. L., and E. T. Walters. 1993b. Activity-dependent depression of mechanosesnsory discharge in *Aplysia*. *J. Neurophysiol.* 70: 1195–1209.

Deuling, H. J., and W. Helfrich. 1991. A theoretical explanation of the myelin shapes of red blood cells. *Blood Cell.* 3:713–720.

Duggan, A. W., P. J. Hope, C. W. Lang, and C. A. Williams. 1991. Sustained isometric contraction of skeletal muscle results in release of immunoreactive neurokinins in the spinal cord of the anaesthesized cat. *Neurosci. Lett.* 122:191–194.

Evans, E. A., and R. Skalak. 1980. Mechanics and Thermodynamics of Biomembranes. CRC Press, Boca Raton, FL.

Firestone, L. L., and R. J. Kitz. 1986. Anesthetics and lipids: some molecular perspectives. *Semin. Anesth.* 5:286–300.

Goldstein, S. S., and W. Rall. 1974. Changes of action potential shape and velocity for changing core conductor geometry. *Biophys. J.* 14:731–757.

Gruner, S. M. 1985. Curvature hypothesis: does the intrinsic curvature determine biomenbrane lipid composition? A role for non-bilayer lipids. *Proc. Natl. Acad. Sci. USA.* 82:3665–3669.

Gruner, S. M., and E. Shyamsunder. 1991. Is the mechanism of general anestesia related to lipid membrane spontaneous curvature? *Ann. N.Y. Acad. Sci.* 625:685–697.

Jackson, M. B., and S. J. Zhang. 1995. Action potential propagation block by GABA in rat posterior pituitary nerve terminals. *J. Physiol. (Lond.).* 483:597–611.

Janmay, P. A., U. Euteneuer, P. Traub, and M. Schliva. 1991. Viscoelastic properties of vimentin compared with other filamentous biopolymer networks. *J. Cell Biol.* 113:155–160.

Janoff, A. S., and K. W. Miller. 1982. A critical assessment of the lipid theories of general anesthetic action. *In:* Biological Membranes. D. Chapman, editor. 4:417–476. Academic Press, New York.

Jensen, J. W., and J. S. Schutzbach. 1988. Modulation of dolichil-phosphomannose synthase activity by changes in the lipid environment of the enzyme. *Biochemistry.* 27:6315–6320.

Katz, B. 1966. Nerve, Muscle and Synapse. McGraw-Hill, New York. 12–51.

Katz, B., and O. Schmitt. 1940. Electrical interactions between two adjacent nerve fibers. *J. Physiol. (Lond.).* 97:471–488.

Katz, B., and O. Schmitt. 1942. A note on interactions between nerve fibers. *J. Physiol. (Lond.).* 100:369–371.

Khodorov, B. I. 1974. The Problem of Excitability: Electrical Excitability and Ionic Permeability of the Nerve Membrane. Plenum, New York.

Kobilka, B. 1992. Adrenergic receptors as models for G protein-coupled receptors. *Annu. Rev. Neurosci.* 15:87–117.

LaMotte, R. H., H. E. Torebjörk, C. J. Robinson, and J. G. Thalhammer. 1984. Time-intesity profile of cutaneous pain in normal and hyperalgesic skin: a comparison with C-fiber nociceptor activities in monkey and human. *J. Neurophysiol.* 51:1434–1450.

Mantyh, P. W., C. J. Allen, J. R. Ghilardi, S. D. Rogers, C. R. Mantyh, H. Liu, A. I. Basbaum, S. R. Vigna, and J. E. Maggio. 1995a. Rapid endocytosis of a G protein-coupled receptor: substance P-evoked internalization of its receptor in the rat striatum in vivo. *Proc. Natl. Acad. Sci. USA.* 92:2622–2626.

Mantyh, P. W., E. DeMaster, A. Malhotra, J. R. Ghilandi, S. D. Rogers, C. R. Mantyh, H. Liu, A. I. Basbaum, S. R. Vigna, J. E. Maggio, and D. A. Simone. 1995b. Receptor endocytosis and dendrite reshaping in spinal neurons after somatosensory stimulation. *Science.* 268:1629–1632.

Markin, V. S., V. F. Pastushenko, and Y. A. Chizmadzhev. 1987a. Theory of Excitable Media. Wiley and Sons, New York.

Markin, V. S., S. Svetina, and B. Zeks. 1987b. Osmotic shrinkage of giant lipid vesicles and the bilayer couple hypothesis (in Russian). *Biol. Membr.* 4:280–289.

Meller, K. 1992. Axoplasmic transport of horseradish peroxidase in single neurons of the dorsal root ganglion studied in vitro by microinjection. *Cell Tissue Res.* 270:139–148.

Morris, C., and H. Lecar. 1981. Voltage oscillation in the barnacle giant muscle fiber. *Biophys. J.* 35:193–213.

Nazif, F. A., J. H. Byrne, and L. J. Cleary. 1991. cAMP induces long-term morphological changes in sensory neurons of *Aplysia*. *Brain Res.* 539: 324–327.

Nelson, P., T. Powers, and U. Seifert. 1995. Dynamic theory of the pearling instability in cylindrical vesicles. *Phys. Rev. Lett.* 74:3384–3387.

Pastushenko, V. F., and V. S. Markin. 1969. Excitation propagation in a model of a nonuniform nerve fiber. *Biofisika.* 14:517–520.

Perl, E. R. 1968. Myelinated afferent fibers innervating the primate skin and their response to noxious stimuli. *J. Physiol. (Lond.).* 197:593–615.

Persiasami, N., M. Armijo, and A. S. Verkman. 1991. Picosecond rotation of small polar fluorophores in the cytosol of sea urchin eggs. *Biochemistry.* 30:11836–11841.

Plateau, J. 1873. Statique Experimentale et Theorique des Liquides Soumis aux Seules Forces Moleculaires. Gautier-Villars, Paris.

Ramon, F., R. W. Joyner, and J. W. Moore. 1975. Propagation of action potential in inhogeneous axon regions. *Fed. Proc.* 34:1357–1363.

Lord Rayleigh. 1964. Scientific Papers, Vol. 1. Dover, New York. 361–371, 379–401.

Rayleigh. 1892. *Philos. Mag.* 34:145.

Rinzel, J., and G. B. Ermentrout. 1989. Analysis of neural excitability and oscillations. *In* Methods in Neural Modeling: From Synapses to Networks. C. Koch and I. Segev, editors. MIT Press, Cambridge, MA.

Salter, M. W., and J. L. Henry. 1991. Responses of functionally identified neurones in the dorsal horn of the cat spinal cord to substance P, neurokinin A and physalaemin. *Neuroscience.* 43:601–610.

Sato, M., W. H. Shwartz, S. C. Selden, and T. D. Pollard. 1988. Mechanical properties of brain tubulin and microtubules. *J. Cell Biol.* 106: 1205–1211.

Seifert, U. 1994. Fluid membranes: theory of vesicle conformations. Thesis. Munich.

Stoltennbury-Didinger, G., F. Boegner, W. Grüning, M. Wagner, P. Marx, and H. Altenkirch. 1992. Specific neurotoxic effects of different organic solvents on dissociated cultures of the nervous system. *Neurotoxicology.* 13:161–164.

Suneson, A., H.-A. Hansson, E. Lycke, and T. Seeman. 1989. Pressure wave injuries to rat dorsal root ganglion cells in culture caused by high-energy missiles. *J. Trauma.* 29:10–18.

Tsai, M. A., R. S. Frank, R. E. Waugh. 1993. Passive mechanical behavior of human neutrophils: power-law fluid. *Biophys. J.* 65:2078–2088.

Walters, E. T. 1987. Multiple sensory neuronal correlates of site-specific secsitization in *Aplysia*. *J. Neurosci.* 7:408–417.

Wang, Z., R. J. Van den Berg, and D. L. Ypey. 1994. Resting membrane potentials and excitability at different regions of rat dorsal root ganglion neurons in culture. *Neuroscience.* 60:245–254.

Wiedmann, T. S., R. D. Pates, J. M. Beach, A. Salmon, and M. F. Brown. 1988. Lipid protein interactions mediate the photochemical functions of rhodopsin. *Biochemistry.* 27:6469–6474.

Wilcox, G. L. 1988. Pharmacological studies of grooming and scratching behavior elicited by spinal substance P and excitatory amino acids. *Ann. N.Y. Acad. Sci.* 525:228–236.